IEEE Photonics Journal
An IEEE Photonics Society Publication

Open Access

Phase Control of Optical Nonreciprocity in Photonic Bandgap Four-Wave Mixing

Volume 8, Number 3, June 2016

Yunzhe Zhang
Irfan Ahmed
Dan Zhang
Zhe Liu
Weitao Zhang
Wenhui Yi
Yanpeng Zhang

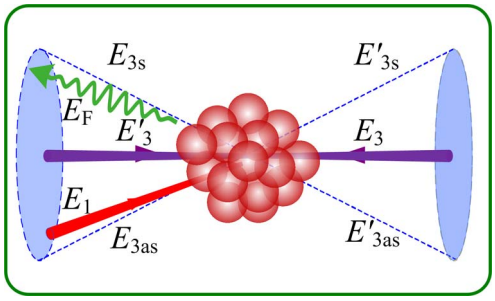

DOI: 10.1109/JPHOT.2016.2551461
1943-0655

IEEE photonics SOCIETY

IEEE

Phase Control of Optical Nonreciprocity in Photonic Bandgap Four-Wave Mixing

Yunzhe Zhang,[1,2] Irfan Ahmed,[1,3] Dan Zhang,[1] Zhe Liu,[2] Weitao Zhang,[2] Wenhui Yi,[1] and Yanpeng Zhang[1]

[1]Key Laboratory for Physical Electronics and Devices of the Ministry of Education and Shaanxi Key Laboratory of Information Photonic Technique, Xi'an Jiaotong University, Xi'an 710049, China
[2]Institute of Applied Physics, Xi'an University, Xi'an 710065, China
[3]Department of Electrical Engineering, Sukkur Institute of Business Administration, Sukkur 65200, Pakistan

DOI: 10.1109/JPHOT.2016.2551461

Manuscript received March 26, 2016; accepted April 2, 2016. Date of publication April 21, 2016; date of current version April 28, 2016. This work was supported in part by the 973 Program under Grant 2012CB921804, by the National Natural Science Foundation of China under Grant 11474228, and by Key Scientific and Technological Innovation Team (KSTIT) of Shaanxi Province (2014KCT-10). Corresponding author: Y. Zhang (e-mail: ypzhang@mail.xjtu.edu.cn).

Abstract: We investigate the optical nonreciprocity induced by the parametrical amplification and the radiation trapping in an atomic photonic bandgap system both theoretically and experimentally. We use two pumping fields to generate entangled photon pairs from spontaneous parametric four-wave mixing, as well as the signals in which they can be enhanced by the feedback dressing effect. Therefore, the frequency difference and the shape change due to this feedback dressing on the two-arm ramps of one round trip are observed. Such optical nonreciprocity can be easily controlled by multiple experimental parameters (frequency detuning, power, and phase) of the dressing beams. In addition, the enhancement and suppression switching induced by the double dressing or triple dressing conditions are also studied. This optical nonreciprocity can contribute to the development of quantum information processing and quantum communications.

Index Terms: Four-wave mixing (FWM), photonic bandgap, optical nonreciprocity.

1. Introduction

Optical nonreciprocity resembles optical bistability, which is common optical properties in atomic media. Optical bistability has been investigated over the last several decades and observed in vaious materials. Along different lines, electromagnetically induced transparency (EIT) [1]–[3] can effectively decrease the absorption of incident beams and has been researched since it may have potential applications in nonlinear optics and wave-mixing processes [4]. Besides, in atomic system, optical bistability plays important role in four-wave mixing (FWM) in thick atomic vapor with two counter-propagating laser beams [5],[6]. If the two laser beams have the same frequency and propagate in the opposite directions, the electromagnetically induced grating (EIG) will be generated in thick atomic vapor [7]–[10], which establishes a photonic band gap (PBG) structure [11], [12]. For thick atomic vapor, radiation trapping that results from the reabsorption of spontaneously emitted photons [13], [14] has also been studied extensively in astrophysics, plasma physics, and atomic spectroscopy [15], [16].

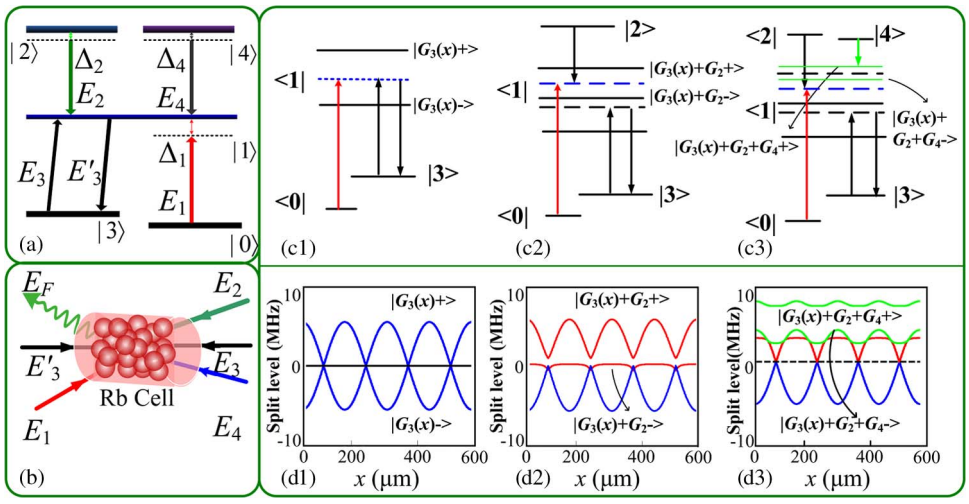

Fig. 1. (a) Five-level energy system. (b) Schematic of a PBG structure (formed by two coupling beams $\boldsymbol{E}_3$ and $\boldsymbol{E}_3'$) dressed by $\boldsymbol{E}_2$ and $\boldsymbol{E}_4$. (c1)–(c3) Dressed energy level schematics. (d1)–(d3) Calculated dressed period energy level.

In addition, a spontaneous parametric FWM (SP-FWM) process generates two weak fields (Stokes field and anti-Stokes field) in a forward cone. With signal filed injected into the Stokes port, the system can experience optical parametrical amplification (OPA) process [17]. Recently, schemes for realizing FWM OPA process have also been experimentally and theoretically studied [18].

In this paper, the optical nonreciprocity characterized as the parametrically amplification or radiation trapping, which is similar to the optical bistable (OB) behavior, has been experimentally observed and discussed for the first time, This optical nonreciprocity refers that the generated signals can not be overlapped when the signals on the rising edge and the falling edge are folded. Meanwhile, the frequency difference and change of shape between the folded signals (the probe transmission signals (PTS), FWM, and fluorescence signals (FLS)) can be observed and effectively controlled by multiple parameters. Moreover, we study the PBG FWM enhancement and suppression switching induced by the double dressing or triple dressing effects.

2. Experimental Setup and Theoretical model

2.1. Experimental Setup

Our experiment is performed in a rubidium atomic cell, and the rubidium cell is wrapped by μ-metal and heated by the heater tape, so we can control the temperature of Rb easily. The relevant energy levels for ^{85}Rb atoms are shown in Fig. 1(a), which is composed by $5S_{1/2}(F=3)(|0\rangle)$, $5S_{1/2}(F=2)(|3\rangle)$, $5P_{3/2}(|1\rangle)$, $5D_{3/2}(|4\rangle)$ and $5D_{5/2}(|2\rangle)$. The probe laser beam $\boldsymbol{E}_1$ (frequency ω_1, wave vector $\boldsymbol{k}_1$ and Rabi frequency G_1) connects $|0\rangle \rightarrow |1\rangle$, coupling laser beams $\boldsymbol{E}_3$ (ω_3, $\boldsymbol{k}_3$ and G_1) and $\boldsymbol{E}_3'$ (ω_3, $\boldsymbol{k}_3'$ and G_3') connect the transition $|3\rangle \rightarrow |1\rangle$, the dressing laser beam $\boldsymbol{E}_2$ (ω_2, $\boldsymbol{k}_2$ and G_2) and $\boldsymbol{E}_4$ (ω_4, $\boldsymbol{k}_4$ and G_4) connect $|1\rangle \rightarrow |2\rangle$ and $|1\rangle \rightarrow |4\rangle$, respectively. Here, $G_i = \mu_i \boldsymbol{E}_i/\hbar$ is the Rabi frequency with transition dipole moment μ_i. As shown in Fig. 1(b), the coupling fields $\boldsymbol{E}_3$ and $\boldsymbol{E}_3'$ propagate through ^{85}Rb vapor in the opposite direction of each other, which will generate a standing wave $E_{31} = \hat{y}[E_3\cos(\omega_3 t - k_3 x) + E_3'\cos(\omega_3' t + k_3' x)]$ [19]. The standing wave will lead to a PBG structure, which will be modified by the dressing fields $\boldsymbol{E}_2$ and $\boldsymbol{E}_4$. Then, the probe field $\boldsymbol{E}_1$ propagating in the same direction of $\boldsymbol{E}_3'$

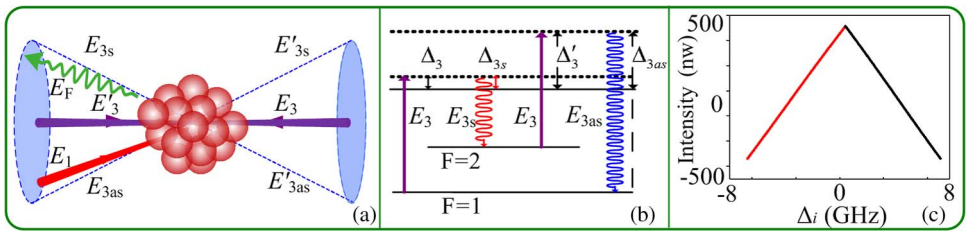

Fig. 2. (a) Phase-matching geometrical diagram of the OPA process. (b) Energy schematic of the FWM OPA process. (c) Two-arm ramps of one round trip and the intensity of the signals changes from 0 to 500 nW. The annotation Δ_i indicates the detuning of the dressing field $\boldsymbol{E}_2$ or $\boldsymbol{E}_4$.

through the ^{85}Rb with a small angle between them, and the dressing fields $\boldsymbol{E}_2$ and $\boldsymbol{E}_4$ propagate in the opposite direction of $\boldsymbol{E}'_3$ with a small angle. According to the phase-matching condition $\boldsymbol{k}_F = \boldsymbol{k}_1 + \boldsymbol{k}_3 - \boldsymbol{k}'_3$, the PBG FWM ($\boldsymbol{E}_F$) and the PTS are detected by a photodiode and an avalanche photodiode detector (APD), respectively. In addition, the FLS caused by spontaneous decay are captured by another photodiode detector. Lastly, the power of each laser beam can be modulated by a polarized beam splitter (PBS) and half-wave plate (HWP), the frequency detuning $(\Delta_i = \Omega_i - \omega_i)$ can be modulated through the laser's piezoelectric transducer (PZT) driver.

In addition, due to the periodicity of the standing wave field, we can obtain the periodic energy levels as displayed in Fig. 1(c). As shown in Fig. 1(c1), $|G_{31}|^2$ splits the level $|1\rangle$ into two substates expressed as $|G_{31}\pm\rangle$, which are periodic along the x direction. The single-dressed case is shown in Fig. 1(c2), where $\boldsymbol{E}_2$ acts as single dressed field on the states $|G_{31}\pm\rangle$ and splits the initial two substates further into secondary dressed states $|G_{31} - G_2\pm\rangle$ and $|G_{31} + G_2\pm\rangle$. For the doubly-dressed case in Fig. 1(c3), when $\boldsymbol{E}_4$ is turned on, $|G_{31} \pm G_2\pm\rangle$ are further split into dressed states $|G_{31} \pm G_2 \pm G_4\pm\rangle$. The corresponding spatial periodic energy levels are shown in Fig. 1(d1)–(d3).

2.2. PTS and PBG FWM With Feedback Dressing

In order to investigate the influence of nonreciprocity in PBG FWM process, we further study an optical parametric amplification (OPA) process as depicted in Fig. 2. In our experiment, when we compare the folded signals on the rising edge and the falling edge (a frequency round trip ranging from –10 GHz to 10 GHz) as shown in Fig. 2(c), we find that these signals have obvious frequency difference and shape change (see Figs. 3–6), and this optical nonreciprocity can be attributed to the OPA process.

First of all, we study the FWM OPA process. When $\boldsymbol{E}_1$, $\boldsymbol{E}_3$ and $\boldsymbol{E}'_3$ are opened, the PBG FWM satisfies the phase matching condition $\boldsymbol{k}_F = \boldsymbol{k}_1 + \boldsymbol{k}_3 - \boldsymbol{k}'_3$. However, if the power of $\boldsymbol{E}_3$ is high enough and it is far detuned from $|0\rangle \rightarrow |1\rangle$, a spontaneous parametric FWM process will occur in the degenerate two-level atomic configuration [see Fig. 2(b)], which generates two weak fields (Stokes field $\boldsymbol{E}_{3S}$ and anti-Stokes field $\boldsymbol{E}_{3as}$) with the phase matching condition $2\boldsymbol{k}_3 = \boldsymbol{k}_{3s} + \boldsymbol{k}_{3as}$ in the left cone [see Fig. 2(a)]. Then, the generated $\boldsymbol{E}_F$ signal is naturally injected into the input Stokes port of the SP-FWM process and it is parametrically amplified in Fig. 2(a) [19]. Second, the $\boldsymbol{E}'_3$ field has a similar effect with $\boldsymbol{E}_3$, which generates two weak fields (Stokes field $\boldsymbol{E}'_3$ and anti-Stokes field $\boldsymbol{E}'_{3as}$), satisfying $2\boldsymbol{k}'_3 = \boldsymbol{k}'_{3s} + \boldsymbol{k}'_{3as}$ in the right cone [see Fig. 2(a)]. Therefore, the PTS will be parametrically amplified in Fig. 2(a). One can clearly see that the PTS and FWM OPA process have a feedback dressing effects, which are held responsible for the optical nonreciprocity phenomenon in our experiment.

Theoretically, considering the feedback dressing effect of the PTS and PBG FWM written as $|G_{FT}|^2 e^{i\varphi_{FT}}$ and $|G_{FR}|^2 e^{i\varphi_{FR}}$, the amplified PTS and PBG FWM can be described by the energy

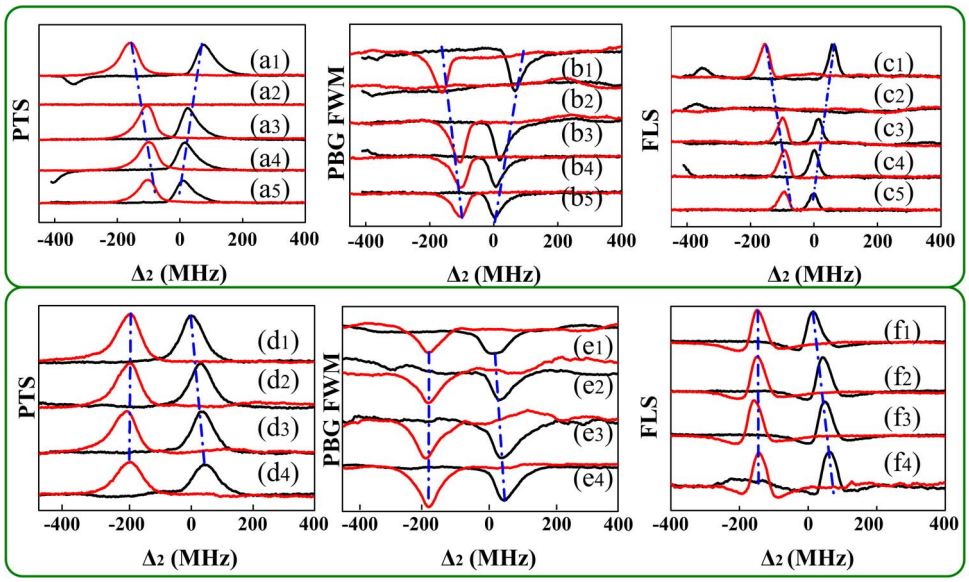

Fig. 3. Measured (a) PTS, (b) PBG FWM, and (c) FLS versus Δ_2 with laser fields (1) all on, (2) $\boldsymbol{E}_1$, (3) $\boldsymbol{E}_3$, (4) $\boldsymbol{E}_3'$, and (5) $\boldsymbol{E}_3$, and $\boldsymbol{E}_3'$ turned off from top to bottom, respectively. Measured (d) PTS, (e) PBG FWM, and (f) FLS versus Δ_2 with $\varphi_2 = 0$ at different discrete Δ_1 as (1) 0, (2) –20, (3) –40, and (4) –60 MHz from top to bottom, respectively.

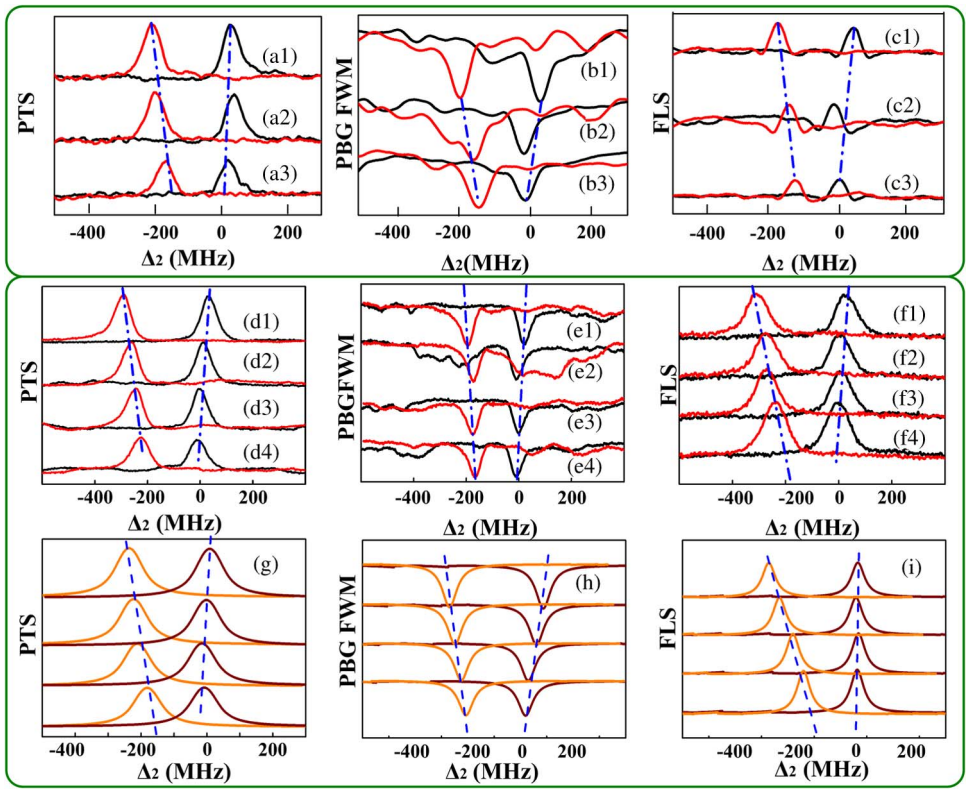

Fig. 4. Measured (a) PTS, (b) PBG FWM, and (c) FLS versus Δ_2 with $\Delta_1 = \Delta_3 = 0$, $\varphi_2 = 0$, and the power of $\boldsymbol{E}_2$ is set as 9.2, 17.1, and 25.7 mW from bottom up, respectively. Measured (d) PTS, (e) PBG FWM, and (f) FLS versus Δ_2 with $\varphi_2 = 0$ and the temperature of ^{85}Rb increases from 42 °C to 63 °C, respectively.

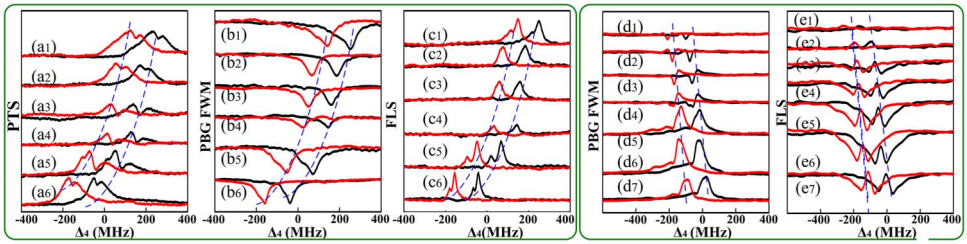

Fig. 5. Measured (a) PTS, (b) PBG FWM, and (c) FLS versus Δ_4 with Δ_1 setting as (1) −250, (2) −200, (3) −150, (4) −80, (5) −40, and (6) 0 MHz, from top to bottom, respectively. Measured (d) PBG FWM and (e) FLS when we change the phase of $\boldsymbol{E}_2$ as (1) $-\pi/6$, (2) $-\pi/3$, (3) $-\pi/2$, (4) $-\pi$, (5), $-7\pi/6$, and (7) $-4\pi/3$, respectively, with $\varphi_4 = 0$ and temperature $T = 60$ °C.

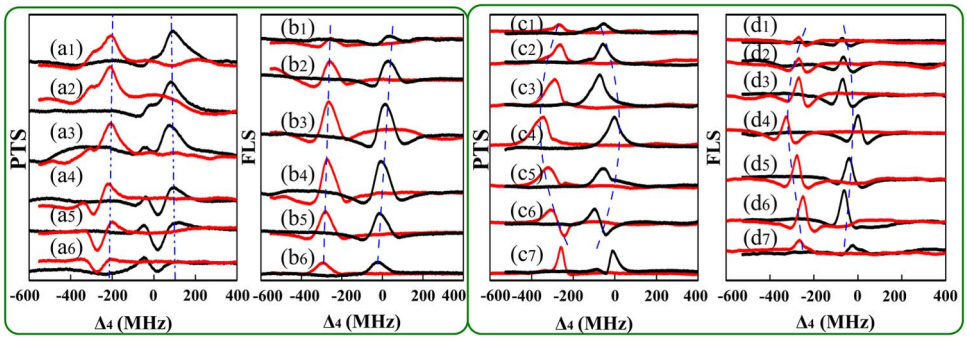

Fig. 6. Measured (a) PTS and (b) FLS versus Δ_4 at $\varphi_2 = \pi/3$, with the phase of $\boldsymbol{E}_4$ setting as (1) π, (2) $2\pi/3$, (3) $\pi/3$, (4) 0, (5) $-\pi/6$, and (6) $-\pi/3$, respectively. Measured (c) PTS, (d) FLS versus Δ_4 at $\varphi_4 = \pi$ with the phase of $\boldsymbol{E}_2$ setting as (1) π, (2) $2\pi/3$, (3) $\pi/3$, (4) 0, (5) $-\pi/6$, (6) $-\pi/3$, and (7) $-\pi/2$, respectively.

system and Liouville pathways, and the corresponding density matrix elements can be written as [20]

$$\rho_{10}^{(1)} = \frac{iG_1}{d_{10} + |G_{31}|^2/d_{30} + |G_2|^2 e^{i\varphi_2}/d_{21} + |G_4|^2 e^{i\varphi_4}/d_{41} d_{10} + |G_{\mathrm{FT}}|^2 e^{i\varphi_{\mathrm{FT}}}/\Gamma_{00}} \tag{1}$$

$$\rho_{10}^{(3)} = \frac{-iG_1 G_3 G_3'}{(d_{10} + |G_{31}|^2/d_{30} + |G_2|^2 e^{i\varphi_2}/d_{21} + |G_4|^2 e^{i\varphi_4}/d_{41} + |G_{\mathrm{FR}}|^2 e^{i\varphi_{\mathrm{FR}}}/\Gamma_{00})^2 d_{30}} \tag{2}$$

where $d_{10} = \Gamma_{10} + i\Delta_1$, $d_{30} = \Gamma_{30} + i\Delta_1 - i\Delta_3$, $d_{21} = \Gamma_{20} + i\Delta_1 + i\Delta_2$, $d_{41} = \Gamma_{40} + i\Delta_1 + i\Delta_4$, $\Delta_1 = \Omega_{10} - \omega_1$, $\Delta_2 = \Omega_{21} - \omega_2$, $|G_{31}|^2 = |G_3|^2 + |G_3'|^2 + 2G_3 G_3' \cos(2k_3 x)$, frequency detuning $\Delta_i = \Omega_i - \omega_i$ (Ω_i is the resonance frequency of the transition driven by $\boldsymbol{E}_i$), $G_{\boldsymbol{F}} = \mu_{\boldsymbol{F}} \boldsymbol{E}_{\boldsymbol{F}}/\hbar$ is the Rabi frequency of the feedback [21]–[23], and Γ_{ij} is transverse relaxation rate between $|i\rangle$ and $|j\rangle$. The feedback dressing on the PTS and FWM OPA process are represented by the term $|G_{\mathrm{FT}}|^2 e^{i\varphi_{\mathrm{FT}}}$ and $|G_{\mathrm{FR}}|^2 e^{i\varphi_{\mathrm{FR}}}$, respectively. Terms φ_2 and φ_4 are the phase factor of the dressing $|G_2|^2 e^{i\varphi_2}/d_{21}$ and $|G_4|^2 e^{i\varphi_4}/d_{41}$. According to the relation $\varepsilon_0 \chi E = N\mu\rho$ (N is the atom density), the susceptibilities can be written as

$$\chi^{(1)} = \frac{iN\mu^2}{\hbar\varepsilon_0} \frac{1}{d_{10} + |G_{31}|^2/d_{30} + |G_2|^2 e^{i\varphi_2}/d_{21} + |G_4|^2 e^{i\varphi_4}/d_{41} d_{10} + |G_{\mathrm{FT}}|^2 e^{i\varphi_{\mathrm{FT}}}/\Gamma_{00}} \tag{3}$$

$$\chi^{(3)} = -\frac{iN\mu^2}{\hbar\varepsilon_0} \frac{1}{(d_{10} + |G_{31}|^2/d_{30} + |G_2|^2 e^{i\varphi_2}/d_{21} + |G_4|^2 e^{i\varphi_4}/d_{41} + |G_{\mathrm{FR}}|^2 e^{i\varphi_{\mathrm{FR}}}/\Gamma_{00})^2 d_{30}}. \tag{4}$$

Moreover, the nonlinear coupled wave equations [24] $\partial E_p(x)/\partial x = -aE_p(x) + ke^{i_\Delta k_x x}E_r(x)$ and $-\partial E_r(x)/\partial x = -aE_r(x) + ke^{-i_\Delta k_x x}E_r(x)$ are given to estimate the reflection efficiency, where $\boldsymbol{E}_p(x)$ and $\boldsymbol{E}_r(x)$ stand for the PTS and PBG FWM signals, respectively. The reflectivity R and transmission T at certain x are given as

$$R = \left|\frac{1}{k}\frac{-e^{\lambda_2^- dx} + e^{\lambda_2^+ dx}}{(\lambda_1^- + \alpha^A)^{-1}e^{\lambda_2^+ dx} - (\lambda_1^+ + \alpha^A)^{-1}e^{\lambda_2^- dx}}\right|^2 \text{ and } T = \left|\frac{e^{(\lambda_1^- + \lambda_1)dx}(\lambda_1^- - \lambda_1^+)}{(\lambda_1^- + \alpha)e^{\lambda_1^- dx} - (\lambda_1^+ + \alpha)e^{\lambda_1^+ dx}}\right|^2$$

where d_x is width of the sample in x direction. $\lambda_1^\pm = -\Delta k_x/2 \pm [(\alpha - i\Delta k_x/2)^2 - k^2]^{1/2}$ and $\lambda_2^\pm = \lambda_1^\pm + i\Delta k_x$, where Δk_x is the phase mismatch magnitude. Take the reflection signals (PBG FWM) as example, the photon numbers of the output Stokes and anti-Stokes fields are $\langle \hat{a}_{\text{out}}^+ \hat{a}_{\text{out}}\rangle = G\langle \hat{a}_{\text{in}} + \hat{a}_{\text{in}}\rangle + (G-1)$ and $\langle \hat{b}_{\text{out}}^+ \hat{b}_{\text{out}}\rangle = (G-1)\langle \hat{a}_{\text{in}}^+ \hat{a}_{\text{in}}\rangle + (G-1)$, where $\hat{a}(\hat{b})$ is the annihilation operator of $\boldsymbol{E}_{3S}(\boldsymbol{E}_{3as})$, and $G = \{\cos[2t\sqrt{AB}\sin(\varphi_1+\varphi_2)/2] + \cosh[2t\sqrt{AB}\cos(\varphi_1 + \varphi_2)/2]\}/2$ is the gain of the process with the modules A and B (phases φ_1 and φ_2) defined as $\rho_{10(st)}^{(1,3)} = Ae^{i\varphi_1}$ and $\rho_{10(\text{ast})}^{(1,3)} = Be^{i\varphi_2}$, respectively. In addition, the parametrically amplified PTS can be discussed in the same way, the photon numbers of the output Stokes and anti-Stokes fields of the OPA are $\langle \hat{a}_{\text{out}}^t \hat{a}_{\text{out}}^+\rangle = G\langle \hat{a}_{\text{in}}^t \hat{a}_{\text{in}}^t\rangle + (G-1)$ and $\langle \hat{b}_{\text{out}}^t \hat{b}_{\text{out}}^t\rangle = (G-1)\langle \hat{a}_{\text{in}}^t \hat{a}_{\text{in}}^t\rangle + (G-1)$, respectively.

2.3. FLS With Feedback Dressing

In our experiment, radiation trapping will occur when light interacts with thick media, and the fluorescence signals (FLS) will be trapped in this process, which also has a feedback dressing effect. Therefore, we can find the optical nonreciprocity phenomenon from the folded FLS. Theoretically, considering the feedback dressing $|G_{\text{FL}}|^2 e^{i\varphi_{\text{FL}}}$ of the FLS, the second-order fluorescence FL_{R1} is described by $\rho_{00}^{(0)} \xrightarrow{E_1} \rho_{10}^{(1)} \xrightarrow{E_1^*} \rho_{11}^{(2)}$. By solving the coupled density-matrix equations, the FL_{R1} is dressed and the expression of $\rho_{11}^{(2)}$ can be modified as

$$\rho_{11}^{(2)} = \frac{-|G_1|^2}{\Gamma_{11}(d_1 + |G_{31}|^2/d_{30} + |G_2|^2 e^{i\varphi_2}/d_{21} + |G_4|^2 e^{i\varphi_4}/d_{41} + |G_{\text{FL}}|^2 e^{i\varphi_{\text{FL}}}/\Gamma_{00})} \tag{5}$$

where $|G_{\text{FL}}|^2 e^{i\varphi_{\text{FL}}}$ is the feedback dressing term by radiation trapping [13]. Via Liouville pathway $\rho_{00}^{(0)} \xrightarrow{E_1} \rho_{10}^{(1)} \xrightarrow{E_2} \rho_{20}^{(2)} \xrightarrow{E_1^*} \rho_{21}^{(3)} \xrightarrow{E_2^*} \rho_{22}^{(4)}$, we can obtain the fourth-order FL_{R2} signal as

$$\rho_{22}^{(4)} = \frac{|G_1|^2|G_2|^2}{(d_{10} + |G_{\text{FL2}}|^2/\Gamma_{00})(d_2 + |G_2|^2 e^{i\varphi_2}/d_{10})d_5\Gamma_2 2} \tag{6}$$

where $d_5 = \Gamma_{21} + i\Delta_2$. Similarly, for the fourth-order fluorescence FL_{R4} with beams $\boldsymbol{E}_2$ and $\boldsymbol{E}_4$ turned on, the FL_{R4} is given as

$$\rho_{44}^{(4)} = \frac{|G_1|^2|G_4|^2}{\Gamma_{44}(d_{10} + |G_2|^2 e^{i\varphi_2}/d_{21} + |G_{\text{FL4}}|^2 e^{i\varphi_{\text{FL}}}/\Gamma_{10})(d_{41} + |G_4|^2 e^{i\varphi_4}/d_{10})d_6}. \tag{7}$$

The intensities of the FLS are $I_{\text{FL}_{R1}} = N\mu\rho_{11}^{(2)}$, $I_{\text{FL}_{R2}} = N\mu\rho_{22}^{(4)}$ and $I_{\text{FL}_{R4}} = N\mu\rho_{44}^{(4)}$, respectively.

2.4. Phase Control of Frequency Difference

Considering OPA and radiation trapping in the above mainly produce an un-neglected feedback dressing $|G_F|^2 e^{i\varphi_F}$ ($|G_{\text{FT}}|^2 e^{i\varphi_{\text{FT}}}$, $|G_{\text{FR}}|^2 e^{i\varphi_{\text{FR}}}$, and $|G_{\text{FL}}|^2 e^{i\varphi_{FL}}$) in the FWM process. The three

signals (PTS, PBG FWM and FLS) have the frequency difference and the shape change. In the following, the optical nonreciprocity phenomena based on frequency difference and the shape change are studied.

Because of OPA or radiation trapping, the folded signals on the rising edge and the falling edge can not overlap. This phenomenon is analogous to the optical bistable behavior. Then the nonreciprocity reflected from the change of nonreciprocal phase $\Delta\varphi$ is as follows:

$$\Delta\varphi = N(n_{2\text{up}} I_{\text{up}} - n_{2\text{down}} I_{\text{down}})\ \omega_p l/c = n_1 \delta l/c \tag{8}$$

δ is the frequency difference, n_1 is the linear refractive index of the Rb cell, and n_2 is the nonlinear refractive index. The feedback intensity I_{up} (or I_{down}) is generated at the same scanning frequency, which is approximately equal to R or T distinctly. Therefore, the frequency difference δ and the intensity of the beam I_{up} and I_{down} are the functions of the probe field $(\boldsymbol{E}_1)$ and the dressing field ($\boldsymbol{E}_2$ and $\boldsymbol{E}_4$), respectively.

Additionally, the suppression and enhancement of these signals play a very important role in the PBG FWM process. For instance when we scanning Δ_2, the primary Autler-Townes (AT) splitting [25] is caused by dressing field $\boldsymbol{E}_2$ and the corresponding eigenvalues are $\lambda_\pm = [\Delta_2 \pm (\Delta_2^2 + 4|G_2|^2\cos(\varphi_2))^{1/2}]/2$, the secondary AT splitting is caused by the feedback dressing term G_F and the corresponding eigenvalues are $\lambda_{+\pm} = [\Delta_2' \pm (\Delta_2' + 4|G_F|^2\cos(\varphi_F))^{1/2}]/2(\Delta_2' = -\Delta_1 - \lambda_+)$. Adjusting $\Delta_2' = 0$ to satisfy the resonance condition, we can get $\lambda_\pm = G'$, and therefore, the split energy levels are $\lambda_+ \pm G_F$ and λ_-. Therefore, the suppression and enhancement conditions of G_2 are $\Delta_1 + \Delta_2 = 0$ and $\Delta_1 + \lambda_\pm = 0$, respectively. With the double feedback dressing effects, the suppression and enhancement conditions are $\Delta_1 + \Delta_2' = 0$ and $\Delta_1 + \lambda_\pm + \lambda_{+\pm} = 0$, respectively. Further, when we scan Δ_4, the split energy levels are $\lambda_+' \pm G_F$ and λ_-', where $\lambda_{++\pm} = [\Delta_2'' \pm (\Delta_2'' + 4|G_4|^2\cos(\varphi_4))^{1/2}]/2$, the suppression and enhancement conditions are $\Delta_1 + \Delta_2'' = 0$ and $\Delta_1 + \lambda_\pm + \lambda_{+\pm} + \lambda_{++\pm} = 0$ with $\Delta_2'' = \Delta_4 - \lambda_+ - \lambda_{++}$.

3. Results and Discussions

According to the experiment results (see Figs. 3–6), we study the nonreciprocity of coexisting PTS, PBG FWM and FLS in detail. The frequency difference (δ) is observed between the rising ramp and falling ramp. The right lines show the signals on the rising ramp and the left ones stand for the signals on the falling edge, and the shape change can be evaluated with the different areas between the signals (right lines and right lines) and the same baseline. Such nonreciprocity behave similarly to the OB effect.

3.1. Double-Dressing Nonreciprocity

Fig. 3 represents nonreciprocity of signals versus scanning detuning Δ_2 with different fields blocked [see Fig. 3(a)–(c)] or different Δ_1 [see Fig. 3(d)–(f)], respectively. First, when $\boldsymbol{E}_1$, $\boldsymbol{E}_3$, and $\boldsymbol{E}_3'$ turned on, the phase matching condition $\boldsymbol{k}_F = \boldsymbol{k}_1 + \boldsymbol{k}_3 - \boldsymbol{k}_3'$ is satisfied, and each peak [Fig. 3(a)] can be seen in the PTS, which denotes that the transparent degree increases, and each peak is the EIT satisfying the $\Delta_1 + \Delta_2 = 0$ and caused by the dressing term $|G_2|^2 e^{i\varphi_2}/d_{21}$ in (1). For frequency difference (δ), because the right peak and left peak in Fig. 3(a1) has the same baseline, the feedback intensity I_{up} is not equal to I_{down} in (8), but $n_{2\text{up}} \approx n_{2\text{down}}$; therefore, (8) can be changed to $\Delta\varphi = Nn_2(I_{\text{up}} - I_{\text{down}})\omega_p l/c = n_1\delta l/c$. It is obvious that δ induces the different I_{up} or I_{down} on the rising edge and the falling edge. Moreover, the feedback intensity I_{up} (I_{down}) has the feedback term $|G_{\text{FT}}|^2 e^{i\varphi_{\text{FT}}}$ so that the δ can be detected on the same baseline in Fig. 3(a). Further, it can be seen that δ decreases from top to bottom in Fig. 3(a), and this phenomenon also can be explained from (8), where n_2 is related to field $\boldsymbol{E}_1$

($\boldsymbol{E}_2$, $\boldsymbol{E}_3$ or $\boldsymbol{E}_3'$) when $(I_{up} - I_{down})$ is fixed and δ is proportional to n_2. It is clear that δ decreases due to the change of n_2 in Fig. 3(a1)–(a5). For example, it can be noticed that δ with all beams on [see Fig. 3(a1)] is bigger than that with beam $\boldsymbol{E}_3$ and $\boldsymbol{E}_3'$ blocked [see Fig. 3(a5)].

Then, we consider the nonreciprocal phase behavior influenced by the feedback dressing in Fig. 3(b). The δ is induced by the feedback term $|G_{FR}|^2 e^{i\varphi_{FR}}$ in (2), and it decreases from top to bottom in Fig. 3(b1)–(b5). In particular, it is clear that δ in the Fig. 3(b1) is the biggest due to the largest n_2. At the same time, for FLS in Fig. 3(c), the δ induced by the feedback term $|G_{FR}|^2 e^{i\varphi_{FR}}$ in (5) decreases from top to bottom in Fig. 3(c1)–(c5).

For corresponding PBG FWM and FLS in Fig. 3(b) and (c), when no beam is blocked in Fig. 3(b1) and (c1), the PBG FWM shows that two digs appear on the baselines in Fig. 3(b1), which are induced by the dressing term $|G_2|^2 e^{i\varphi_2}/d_{21}$ in (2). Each dip shows the PBG FWM related to R in (2) from reflection of the PBS structure. In Fig. 3(c1), the FLS is a sum of $(\rho_{11}^{(2)} + \rho_{22}^{(4)})$, the emission peak $(\rho_{22}^{(4)})$ represents the fourth-order FL_{R2} induced by fields $(E_1 + E_2)$ in (6), and the background signal $(\rho_{11}^{(2)})$ is the second-order FL_{R1} induced by fields $\boldsymbol{E}_1$ $(\boldsymbol{E}_3, \boldsymbol{E}_3')$ in (5). Comparing Fig. 3(c1) with Fig. 3(c5), we find that the emission peak becomes lower in Fig. 3(c5) due to the term $|G_{31}|^2/d_{30}$ in (5). When $\boldsymbol{E}_1$ is blocked, no signal can be detected in Fig. 3(a2)–(c2) because the phase matching condition $\boldsymbol{k}_F = \boldsymbol{k}_1 + \boldsymbol{k}_3 - \boldsymbol{k}_3'$ is not satisfied. For the same reason, when the beams are turned on except $\boldsymbol{E}_3$ or $\boldsymbol{E}_3'$, the PTS decreases obviously, and the PBG FWM disappears in Fig. 3(b3) and (b4). Meanwhile, the peak in FLS also becomes smaller in Fig. 3(c3) and (c4). When $\boldsymbol{E}_3$ and $\boldsymbol{E}_3'$ are blocked, the intensities of the PTS and FLS become smallest in Fig. 3(a5) and (c5), and the dip of PBG FWM becomes the shallowest in Fig. 3(b5) because the term $|G_{31}|^2/d_{30}$ is disappeared in (2). From Fig. 3(a)–(c), the input intensities I_{in}, I_{FL}, R and T can be obtained, which satisfy energy conservation $(I_{FL} + R + T)/I_{in} = 1$.

Especially, when $\boldsymbol{E}_3$ is blocked in Fig. 3(a3), a peak (on one ramp) comes from the second order nonlinearity effect which can be called electromagnetically induced gain. In this case, the beam $\boldsymbol{E}_3'$ becomes a weak probe laser beam, which probes the transition $|3\rangle \rightarrow |1\rangle$. Meanwhile, $\boldsymbol{E}_2$ connects the upper transition $|1\rangle \rightarrow |2\rangle$ with the condition $\Delta_3 + \Delta_2 = 0$. Generally, the density matrix element $\rho_{23}^{(2)}$ can be obtained via the perturbation chain $\rho_{33}^{(0)} \xrightarrow{\omega_3'} \rho_{13}^{(1)} \xrightarrow{\omega_2} \rho_{23}^{(2)}$, we have $\rho_{23}^{(2)} = -G_2 G_3'/(d_{13} + |G_1|^2/d_{03} + |G_2|^2/d_{23} + |G_{31}|^2/\Gamma_{33} + |G'|^2/\Gamma_{33})d_{23}$. Similarly to Fig. 3(b3), beam $\boldsymbol{E}_2$ probes the upper transition $|1\rangle \rightarrow |2\rangle$ while $\boldsymbol{E}_1$ connects the lower transition $|0\rangle \rightarrow |1\rangle$. As the condition $\Delta_1 + \Delta_2 = 0$ is satisfied, the EIA dip appears in Fig. 3(b3). Via the perturbation chain $\rho_{00}^{(0)} \xrightarrow{\omega_1} \rho_{10}^{(1)} \xrightarrow{\omega_2} \rho_{20}^{(2)}$, we have $\rho_{20}^{(2)} = -G_1 G_2/[d_{10} + |G_{31}'|^2/d_{31} + |G_2|^2/d_{21} + |G'|^2/\Gamma_{33}]d_{21}$. Therefore, when the beam $\boldsymbol{E}_3'$ is blocked, the peak (dip) can be seen in Fig. 3(a4)–(b4).

On the other hand, we investigate the optical nonreciprocal behavior affected by double dressing $|G_F|^2 e^{i\varphi_F}$ and $|G_2|^2 e^{i\varphi_2}/d_{21}$ with different Δ_1 as shown in Fig. 3(d)–(f), respectively. For PTS, Fig. 3(d) presents that the EIT peak increases gradually due to different Δ_1 in the $d_{21} = \Gamma_{20} + i\Delta_1 + i\Delta_2$. For PBG FWM, a dip is induced by $\boldsymbol{E}_2$ in Fig. 3(e) because of the dressing term $|G_2|^2 e^{i\varphi_2}/d_{21}$. For the FLS in Fig. 3(f), the dip gradually becomes shallower with Δ_1 setting far from resonance gradually, which is corresponding to the weakening process of EIT. On the contrary, the peak in the dip is FL_{R2} gets stronger with Δ_1 increasing because the FL_{R2} is suppressed due to the dressed term $d_2 + |G_2|^2 e^{i\varphi_2}/d_{10}$ in (6).

Finally, in the Fig. 3(d)–(f), the δ decreases slowly from bottom to top. These experimental phenomena can be explained by the reasons similarly to those Fig. 3(a)–(c). Since n_2 is a function of Δ_1, with $\Delta\varphi = Nn_2(I_{up} - I_{down})\omega_p l/c = n_1 \delta l/c$, δ changes with Δ_1 while $(I_{up} - I_{down})$ is fixed. Especially, in Fig. 3(f3) and (f4), comparison of the areas between the two signals with the same baseline, one can see that the left dip is wider and deeper than the right one due to different $e^{i\varphi_{FL}}$ in the feedback term $|G_{FL}|^2 e^{i\varphi_{FL}}$.

In Fig. 4, we concentrate on the optical nonreciprocity with doubly dressing ($|G_F|^2 e^{i\varphi_F}$ and $|G_2|^2 e^{i\varphi_2}/d_{21}$) effect by changing the power of $\boldsymbol{E}_2$ ((a)–(c)) and the temperature of the rubidium (^{85}Rb) atomic vapor ((d)–(f)). From bottom up, δ increases gradually as shown in Fig. 4(a)–(c), because n_2 is function of the power of $\boldsymbol{E}_2$. In particular, owing to different $e^{i\varphi_{FR}}$ in $|G_{FR}|^2 e^{i\varphi_{FR}}$, we can see that the left dip is deeper than the right dip in Fig. 4(b2) and (b3). Further, when the power of $\boldsymbol{E}_2$ becomes 9.2 mW [see Fig. 4(b1)], the dip profile is asymmetric and the left dip is deeper than the right one. For the PBG FWM in Fig. 4(b), a dip appears in every curve when the double suppression condition $\Delta_1 + \lambda_\pm + \lambda_{+\pm} = 0$ is satisfied. The suppression dip becomes deeper with increasing power duo to the enhanced dressing effect of $\boldsymbol{E}_2$ in Fig. 4(b1)–(b3). In Fig. 4(c), the enhancement peak in each curve becomes bigger with increasing the power of $\boldsymbol{E}_2$.

Next, as temperature affects the density $\boldsymbol{N}$, we analyze nonreciprocal behavior when the temperature of Rb is sufficiently high to reveal its feedback dressing. In Fig. 4(d)–(f), it can be seen that δ increases slowly from bottom up, as it is associated with the term $N\,(n_{2up} l_{up} - n_{2down} l_{down})$ according to (8). If the temperature was set to 63 °C, the left peak (EIT) is taller than the right peak in Fig. 4(d1) because of the different $e^{i\varphi_F}$ in the term $|G_{FR}|^2 e^{i\varphi_{FR}}$. Further, the intensity of PTS is proportional to the equation $P^{(1)} = N\mu\rho_{10}^{(1)}$, and therefore, the height of EIT for PTS increases from small to large as shown in Fig. 4(d1)–(d4). For the PBG FWM shown in Fig. 4(e), the depth of the suppression signal increases from shallow to deep following the equation $P^{(3)} = N\mu\rho_{10}^{(3)}$. With similar reasons, the intensity of the FLS increases from weak to strong as shown in Fig. 4(f) because of $I_{FL_{R1}} = N\mu\rho_{11}^{(2)}$ and $I_{FL_{R2}} = N\mu\rho_{22}^{(4)}$. Fig. 4(g)–(i) are the corresponding theoretical results, which agree with the experimental results in Fig. 4(d)–(f).

3.2. Triple-Dressing Nonreciprocity

In Fig. 5, we focus on optical nonreciprocity with triple dressing by changing Δ_2 (see Fig. 5(a)–(c)) and phase of $\boldsymbol{E}_2$ (see Fig. 5(d)–(e)), where the triple dressing ($|G_F|^2 e^{i\varphi_F}$, $|G_4|^2 e^{i\varphi_4}/d_{41}$ and $|G_2|^2 e^{i\varphi_2}/d_{21}$) are considered. First, in Fig. 5(a), with $\boldsymbol{E}_1$, $\boldsymbol{E}_3$, $\boldsymbol{E}_3'$, $\boldsymbol{E}_2$ and $\boldsymbol{E}_4$ turned on, we study the signals by scanning Δ_4 at different Δ_1. The peaks (EIT) are the dressed PTS induced by the third level dressing effect of $\boldsymbol{E}_4$, and the two-photon resonance condition $\Delta_4 = -\Delta_1$ that determines the two-photon dressing term $|G_2|^2 e^{i\varphi_2}/d_{21} + |G_4|^2 e^{i\varphi_4}/d_{41}$ is satisfied in Fig. 5(a). Especially, it can be see that each EIT peak has two small peaks in Fig. 5(a) due to AT splitting. This phenomenon can be explained as the secondary dressed states $|G_{31} \pm G_2 \pm\rangle$ are split into tertiary dressed states $|G_{31} \pm G_2 \pm G_4 \pm\rangle$ [see Fig. 1(c3)]. For PBG FWM, dip appears in each curve due to $|G_4|^2 e^{i\varphi_4}/d_{41}$ in (2). Because of the interplay between $\boldsymbol{E}_2$ and $\boldsymbol{E}_4$, the suppression dip is the shallowest at $\Delta_4 = -\Delta_1$. Based on the similar method, we can find that the emission peak in each curve is the FL_{R4} signal related to $\rho_{44}^{(4)}$ in (7). At the resonance point $\Delta_4 = -\Delta_1$, the intensity of the peak is the smallest due to the term $d_1 + |G_4|^2/d_{41}$ in (5).

For optical nonreciprocal phenomenon, One can see that change of δ is not obvious in Fig. 5(a)–(c), but the term $e^{i\varphi_{FR}}$can influence the shape of signals, and therefore, the linewidth of left dip in Fig. 5(b5) is about 90 MHz which is much wider than that in Fig. 5(b4).

Then, we especially focus on the phase (φ_2) modulation on the PBG FWM [see Fig. 5(d)] and FLS [see Fig. 5(e)]. When the dressing beam $\boldsymbol{E}_2$ shifts with a small phase (φ_2) from its normal directions, the behavior of the detected signal will change significantly, and it could be manipulated by the orientations of induced dipole moments. For the PBG FWM, the switch between the suppression and enhancement appears in Fig. 5(d), because the suppression and enhancement conditions under the triply dressing condition are $\Delta_1 + \Delta_2'' = 0$ and $\Delta_1 + \lambda_\pm + \lambda_{+\pm} + \lambda_{++\pm} = 0$ with $\Delta_2'' = \Delta_4 - \lambda_+ - \lambda_{++}$. It is clear that the suppression-enhancement switch of PBG FWM is reflected in the variation in signal's intensity with different φ_2. For instance, the enhancement peak of PBG FWM can be detected when $\varphi_2 = -\pi/6$ in Fig. 5(d1), and with φ_2 altered to $-\pi/2$ (or $-\pi$) in [see Fig. 5(d3) or (d4)], the partial suppression dip and the partial enhancement peak

can be detected, then turn to pure enhancement peak with $\varphi_2 = -7\pi/6$ in Fig. 5(d5). Finally, the enhancement peak of PBG FWM reaches its maximum when $\varphi_2 = -7\pi/6$ in Fig. 5(d5). For FLS in Fig. 5(e), with $\varphi_2$changing, the suppression dips FL_{R1} $(\rho_{11}^{(2)})$ change from shallow to deep in the beginning, and then changes to shallow again, as shown in Fig. 5(e1)–(e4). When $\varphi_2 = -7\pi/6$, the suppression dip is the deepest in Fig. 5(e6). The peaks in the dips represent FL_{R4} $(\rho_{44}^{(4)})$, and the peaks get higher and then get shallower with φ_2 changing from $-\pi/6$ to $-4\pi/3$, as shown in Fig. 5(e1)–(e7).

On other hand, δ decreases slowly from bottom up from in Fig. 5(d) and (e). In addition, one can see that the feedback term $|G_{FR}|^2 e^{i\varphi_{FR}}$ affects the switch between the suppression and enhancement of PBG FWM in Fig. 5(d). For example, the left line in Fig. 5(d2) has a suppression dip and two small enhancement peaks.

In this section, we investigate the optical nonreciprocity modulated by two phases φ_2 and φ_4 with the triple dressing effects considered. Comparing Fig. 6(a) and (b) with Fig. 6(c) and (d), the striking difference is that the δ changes from small to big and then decreases in Fig. 6(c) and (d) from bottom up by changing φ_2 (fixing $\varphi_4 = \pi$). However, the change of δ in Fig. 6(a) and (b) is not obvious by changing φ_4 (fixing $\varphi_2 = \pi/3$). Then, we turn to the PTS, the EIT (peak) and EIA (dip) switching can be seen in Fig. 6(a) and (c). For example, when we fix $\varphi_2 = \pi/3$, the PTS is converted from EIA [see Fig. 6(a6)] to partial-EIT and partial-EIA [see Fig. 6 (a5–a4)] and finally to EIT [see Figs. 6(a3–a1)] along the increasing of φ_4. The reason of such switch between EIT and EIA is that the dressing effect gets modulated as φ_4 altered.

Finally, from these experimental results (Figs. 3–6), we can find some differences of the optical nonreciprocity between double dressing (see Figs. 3 and 4) and triple dressing (see Figs. 5 and 6). It is clear that such nonreciprocal enhancement-suppression switching in triply-dressed system is more obvious than in doubly-dressed system. For example, in Figs. 3 and 4 EIT peaks in PTS and suppression dips in PBG FWM with double dressing can be seen, while double small peaks [see Fig. 5(a)], the EIT-EIA switch [see Fig. 6(a) and (c)] in PTS, and the enhancement-suppression switching [see Fig. 5(e)] in PBG FWM are observed under triple dressing case.

4. Conclusion

In summary, we have experimentally presented results that show the optical nonreciprocity of the PBG FWM processes in a thermal rubidium atomic vapor cell, in which the frequency difference and the shape change can be detected from parametrically amplification (PTS, PBG FWM) or the radiation trapping (FLS). Further, we can control the frequency difference and shape change in this nonreciprocity process by easily manipulating the corresponding parameters (the frequency detuning, the powers, the temperature of atoms and the phase) of the dressing beams. Particularly, the switch between EIT and EIA had been observed by changing the phase difference. Besides, by comparing the optical nonreciprocity under double dressing and triple dressing cases, we find the degree of shape change by triple dressing is more sensitive than double dressing. Such nonreciprocity could be used in amplification processing of triode and quantum information processing.

References

[1] Y. P. Zhang, A. W. Brown, and M. Xiao, "Opening four-wave mixing and six-wave mixing channels via dual electromagnetically induced transparency windows," *Phys. Rev. Lett.*, vol. 99, no. 12, Sep. 2007, Art. no. 123603.
[2] C. B. Li *et al.*, "Observation of enhancement and suppression in four-wave mixing processes," *Appl. Phys. Lett.*, vol. 95, no. 4, Jul. 2009, Art. no. 041103.
[3] S. E. Harris, "Electromagnetically induced transparency," *Phys. Today*, vol. 50, no. 7, pp. 36–42, Jul. 1997.
[4] M. Xiao, Y. Q. Li, S. Z. Jin, and J. Gea-Banacloche, "Measurement of dispersive properties of electromagnetically induced transparency in rubidium atoms," *Phys. Rev. Lett.*, vol. 74, no. 5, pp. 666–669, Jan. 1995.
[5] T. Yabuzaki, T. Okarnoto, M. Kitano, and T. Ogawa, "Optical bistability with symmetry breaking," *Phys. Rev. A*, vol. 29, no. 4, pp. 1964–1972, Apr. 1994.

[6] A. S. Novikova, D. F. Zibrov, Phillips, and R. L. Walsworth, "Dynamic optical bistability in resonantly enhanced Raman generation," *Phys. Rev. A*, vol. 69, no. 6, Jun. 2004, Art. no. 061802.
[7] Y. P. Zhang *et al.*, "Four-wave mixing dipole soliton in laser-induced atomic gratings," *Phys. Rev. Lett.*, vol. 106, no. 9, Mar. 2011, Art. no. 093904.
[8] H. Y. Ling, Y. Q. Li, and M. Xiao, "Electromagnetically induced grating: Homogeneously broadened medium," *Phys. Rev. A*, vol. 57, no. 2, pp. 1338–1344 Feb. 1998.
[9] M. Bajcsy, A. S. Zibrov, and M. D. Lukin, "Stationary pulses of light in an atomic medium," *Nature*, vol. 426, no. 6967, pp. 638–641, Dec. 2003.
[10] A. W. Brown and M. Xiao, "All-optical switching and routing based on an electromagnetically induced absorption grating," *Opt. Lett.*, vol. 30, no. 7, pp. 699–701, Apr. 2005.
[11] D. W. Wang *et al.*, "Optical diode made from a moving photonic crystal," *Phys. Rev. Lett.*, vol. 110, no. 9, Feb. 2013, Art. no. 093901.
[12] Y. Q. Zhang *et al.*, "Photonic Floquet topological insulators in atomic ensembles," *Laser Photon. Rev.*, vol. 9, no. 3, pp. 331–338, May 2015.
[13] A. B. Matsko, I. Novikova, M. O. Scully, and G. R. Welch, "Radiation trapping in coherent media," *Phys. Rev. Lett.*, vol. 87, no. 13, Sep. 2001, Art. no. 133601.
[14] A. F. Molisch and B. P. Oehry, *Radiation Trapping in Atomic Vapours*. Oxford, U.K.: Clarendon, 1998.
[15] G. Ankerhold, M. Schiffer, D. Mutschall, T. Scholz, and W. Lange, "Nonlinear effects of radiation trapping in ground-state oriented sodium vapor," *Phys. Rev. A*, vol. 48, no. 6, pp. 4031–4034, Dec. 1993.
[16] W. Happer, "Optical pumping," *Rev. Mod. Phys.*, vol. 44, pp. 169–249, Apr. 1972.
[17] Z. Y. Zhang *et al.*, "Dressed gain from the parametrically amplified four-wave mixing process in an atomic vapor," *Sci. Rep.*, vol. 5, Oct. 2015, Art. no. 15058.
[18] H. B. Zheng *et al.*, "Parametric amplification and cascaded-nonlinearity processes in common atomic system," *Sci. Rep.*, vol. 3, May 2013, Art. no. 01885.
[19] Z. Ullah *et al.*, "Observation of the four wave mixing photonic band gap signal in electromagnetically induced grating," *Opt. Exp.*, vol. 22, no. 24, pp. 29544–29553, Nov. 2014.
[20] P. Y. Li, Z. Y. Zhao, Z. G. Wang, Y. Q. Zhang, and H. Y. Lan, "Phase control of bright and dark states in four-wave mixing and fluorescence channels," *Appl. Phys. Lett.*, vol. 101, no. 8, Aug. 2012, Art. no. 081107.
[21] J. Che *et al.*, "Rydberg dressing evolution via Rabi frequency control in thermal atomic vapors," *Phys. Chem. Chem. Phys.*, vol. 16, pp. 18840–18847, Jul. 2014.
[22] K. J. Boller, A. Imamolu, and S. E. Harris, "Observation of electromagnetically induced transparency," *Phys. Rev. Lett.*, vol. 66, no. 20, pp. 2593–2596, May 1991.
[23] Y. Wu and X. Yang, "Electromagnetically induced transparency in V-, Λ-, and cascade-type schemes beyond steady-state analysis," *Phys. Rev. A*, vol. 71, no. 12, May 2004, Art. no. 053806.
[24] R. L. Abrams and R. C. Lind, "Degenerate four-wave mixing in absorbing media," *Opt. Lett.*, vol. 2, no. 4, pp. 94–96, Dec. 1978.
[25] S. Sang *et al.*, "Observation of angle switching of dressed four-wave mixing image," *IEEE Photon. J.*, vol. 4, no. 5, pp. 1973–1986, Oct. 2012.